Finite-Element Analysis of Dielectric Waveguides with Curved Boundaries

DANIEL WELT AND JON WEBB, MEMBER, IEEE

Abstract—**The modes of dielectric waveguides with curved boundaries are computed efficiently using a curved-sided (isoparametric) second-order finite element rather than the more usual triangular element. A novel way of placing the virtual boundary is described. Results are obtained for dielectric rod and elliptical waveguides, and compared with earlier results. The method is used to analyze a single-mode fiber-optical coupler.**

I. Introduction

THE ACCURATE ANALYSIS of single-mode dielectric waveguides requires the determination of the first few propagating modes. For an arbitrarily shaped guide cross section, numerical methods must be used. This paper describes a finite-element method using quadratic elements with curved sides, well suited to dielectric waveguides with curved boundaries.

The authors who previously developed finite-element techniques for electromagnetic-wave propagation analysis [1]–[7] chose standard triangular elements with linear [1], [3] or high-order interpolation polynomials [2], [5]. Such elements were well adapted to microwave rectangular waveguides [1], [2] or integrated optics applications [3]–[5], [7] but not to optical fibers and related components.

Recently, P. Daly [8] proposed curvilinear elements to solve propagation problems in elliptical and parabolic waveguides, but with a method and a choice of elements limited to these two particular cases.

Our selection of elements with quadratic boundaries has the following advantages.

- Only one type of element can accurately model straight or curved dielectric boundaries.
- The match with straight or quadratic boundaries is perfect.
- The match with circular or elliptical boundaries is excellent.

As it will be shown in the results given later in Section III, the quality of the boundary matching will give excellent accuracy with a relatively small number of elements and a problem of a size compatible with minicomputer capacities.

Manuscript received August 24, 1984; revised February 11, 1985. This work was supported in part by the Natural Sciences and Engineering Research Council of Canada, and in part by the "Fonds F. C. A. C. pour l'aide et le soutien à la Recherche" of Quebec.

D. Welt is with MPB Technologies Inc., 1725 North Service Road, Trans-Canada Highway, Dorval, Québec, Canada H9P 1J1.

J. Webb is with the Electrical Engineering Department, McGill University, 3480 University Street, Montréal, Québec, Canada H3A 2A7.

II. Finite-Element Formulation

As proved in [9], and stated in [1]–[4], the solution of the time-harmonic Maxwell's equations can be written for each mode in a variational form as

$$\delta \sum_{i=1}^{N} \left\{ \int_{S_i} \tau_i |\nabla_t \phi_i|^2 + \gamma^2 \tau_i \left(\frac{\epsilon_i}{\epsilon_0}\right) |\nabla_t \psi_i|^2 + 2\gamma^2 \tau_i \hat{z} \cdot (\nabla_t \psi_i \times \nabla_t \phi_i) + k_0^2 |\phi_i|^2 + k_0^2 \gamma^2 \left(\frac{\epsilon_i}{\epsilon_0}\right) |\psi_i|^2 \, dS_i \right\} = 0 \quad (1)$$

where

N = number of regions in the $x-y$ plane,
i = index of a region (each region must be homogeneous, i.e., ϵ_i is constant),
S_i = area of a region i ($\sum_{i=1}^{N} S_i = S$ = cross section of the domain of integration),

$$\tau_i = \frac{\gamma^2 - 1}{\gamma^2 - \left(\frac{\epsilon_i}{\epsilon_0}\right)} \quad (2)$$

γ = normalized propagation constant = $\beta c/\omega$,
β = propagation constant,
(Any field component f propagating in the $+z$ direction has a z-t dependance of the form $e^{j(\omega t - \beta z)}$.)
ϵ_i/ϵ_0 = relative permittivity in region i,
ϵ_0 = free-space permittivity,

$$k_0^2 = \left(\frac{\omega a}{c}\right)^2 (\gamma^2 - 1) \quad (3)$$

ω = angular frequency of the propagating wave,
a = a normalizing dimension,
c = speed of light in vacuum,
$\phi_i = H_z^i$ = z-component of $\vec{H}$ field in region i,
$\psi_i = \frac{1}{\gamma \eta_0} E_z^i$, E_z^i is the z-component of $\vec{E}$-field in region i,
η_0 = free-space inpedance = μ_0/ϵ_0,
μ_0 = free-space permeability,
$\nabla_t = (\partial/\partial x, \partial/\partial y)$ = vectorial operator.

ϕ_i and ψ_i are functions of the space coordinates $(x-y)$, $x-y$ being defined as the Cartesian coordinates of the cross-section plane.

0018-9480/85/0700-0576$01.00 ©1985 IEEE

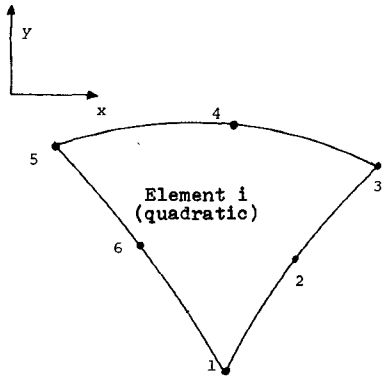

Fig. 1. A typical quadratic element.

The normalized frequency s is defined as

$$s = \frac{\omega a}{c}. \tag{4}$$

For a given value of γ, and a known distribution of the dielectric material in the waveguide cross section, a pair of scalar two-dimensional functions $\{\phi_i, \psi_i\}$ for each region and the common value of k_0^2 constitutes one eigensolution of (1).

It is important to note that the usual field-matching conditions at the inter-region interface (continuity of tangential $\vec{E}$ and $\vec{H}$ fields; continuity of normal $\vec{D}$ and $\vec{B}$ fields) are automatically satisfied when (1) is solved exactly (see [9]).

When the value of γ is between the minimum and the maximum of $\sqrt{\epsilon_i/\epsilon_0}$, an infinite number of discrete and real solutions (the propagating modes) exist. Each one propagates at a different frequency and defines a complete set of six field components. The transverse components, if required, may be simply deduced from the longitudinal components [9].

When the regions i are small enough, it is possible to approximate the solution with polynomial interpolation functions—this is the finite-element method. Therefore, these regions are called "elements."

In order to be able to model arbitrary curved shapes, each element has only three sides, defined by three quadratics and three points, as shown in Fig. 1. Therefore, six points define the geometry of an element.

The search for continuous functions (ϕ_i, ψ_i) is transformed into the search for discrete values at the six nodes through the discretization process widely documented in the finite-element literature [10], [11]. By assuming that ϕ_i and ψ_i can be interpolated in each element from the knowledge of the nodal values, the integrations in (1) can be replaced by the integration of known interpolation functions [10], which become the weights of the unknown nodal values.

In each element i, we can write

$$\phi_i = \sum_{j=1}^{6} N_j \phi_{ij} \tag{5}$$

$$\psi_i = \sum_{j=1}^{6} N_j \psi_{ij} \tag{6}$$

where

$$N_1 = -(1-\xi-\eta)(1-2(1-\xi-\eta)) \tag{7}$$

$$N_2 = 4\xi(1-\xi-\eta) \tag{8}$$

$$N_3 = -\xi(1-2\xi) \tag{9}$$

$$N_4 = 4\xi\eta \tag{10}$$

$$N_5 = -\eta(1-2\eta) \tag{11}$$

$$N_6 = 4\eta(1-\xi-\eta). \tag{12}$$

ξ, η are the local coordinates in the reference triangle.

Theoretically, even if the region of integration should be he entire $x-y$ plane, the fast decay rate of the electromagnetic field outside the waveguide allows an integration over a finite domain limited by the so-called "virtual boundary."

It is also possible to use the symmetry conditions to reduce the size of the integration area by imposing the proper boundary conditions on the axes.

Finally, it may be proved [9], [12] that the final form of (1) after discretization is an eigenvalue problem

$$[A]\{\theta\} + k_0^2[B]\{\theta\} = 0 \tag{13}$$

where

$[A]$ = large–sparse–indefinite–symmetric matrix,
$[B]$ = large–sparse–positive definite–symmetric matrix,
$\{\theta\}$ = a vector containing all the nodal values of ϕ_i and ψ_i.

The parameter γ is present in the matrices $[A]$ and $[B]$. The values k_0^2 are the positive eigenvalues corresponding to the propagating modes. Since $[A]$ is indefinite, negative eigenvalues exist, but are ignored.

III. Test Results

A set of computer programs has been written to carry out a finite-element analysis of dielectric waveguides. Three examples were selected to demonstrate the most important characteristics of the method and to validate the software implementation. The results are given in this section.

A. The Dielectric Rod Example

An infinitely long circular cylinder, with an index of refraction n_1, is embedded in a region of index n_2 (n_1 is greater than n_2). The analytical solution of this problem can be found in many references [12].

An example was chosen with $n_1 = 1.50$ and $n_2 = 1.00$. One quarter of the rod and the surrounding medium were discretized with 50 elements and 129 nodes. It was not necessary to discretize the full plane because of the symmetric geometry of the system.

Tables I and II give the numerical results and the corresponding errors for the normalized frequency s as a function of the normalized propagation constant γ. This error is below 0.035 percent over the γ-range (1.05–1.49) for the dominant HE_{11} mode. The $\phi(H_z)$- and $\psi(E_z)$-field components for $\gamma = 1.45$ are shown in Fig. 2. The number denoted N_0 in Tables I and II indicates an ordering of the computed positive eigenvalues, starting from the smallest.

TABLE I
THE DIELECTRIC ROD EXAMPLE: HE_{11} AND HE_{12} MODES

HE_{11}					HE_{12}				
γ	S (Th.)	No*2	S (FEM)*1	% Error	γ	S (Th.)	No*2	S (FEM)*1	% Error
1.05	1.290371	1	1.290175	-.015	1.05	3.71919	2	3.72199	+.075
1.10	1.510383	1	1.510468	+.006	1.10	4.02084	2	4.02389	+.076
1.15	1.71591	2	1.71619	+.016	1.15	4.36556	3	4.36900	+.079
1.20	1.938383	1	1.938836	+.023	1.20	4.78074	2	4.78424	+.073
1.25	2.20246	1	2.20302	+.026	1.25	5.30594	2	5.30988	+.074
1.30	2.54322	1	2.54397	+.030	1.30	6.01055	2	6.01514	+.076
1.35	3.02859	1	3.02956	+.032	1.35	7.03786	3	7.04330	+.077
1.40	3.83111	1	3.83237	+.033	1.40	8.75663	2	8.76278	+.070
1.45	5.63521	2	5.63680	+.028	1.45	12.6354	3	12.6440	+.068
1.46	6.36240	2	6.36446	+.032	1.46	14.1989	3	14.2074	+.060
1.47	7.42959	1	7.43224	+.036	1.47	16.4904	3	16.5036	+.080
1.48	9.22224	1	9.22550	+.035	1.48	20.3352	3	20.3491	+.069
1.49	13.2758	1	13.2804	+.035	1.49	29.0159	3	29.0342	+.063

*1 FEM solution with 50 elements and 129 nodes.
*2 Eigenvalue number.

TABLE II
THE DIELECTRIC ROD EXAMPLE: HE_{21} AND HE_{22} MODES

HE_{21}					HE_{22}				
γ	S (Th.)	No*2	S (FEM)*1	% Error	γ	S (Th.)	No*2	S (FEM)*1	% Error
1.05	2.78442	2	2.7533	-1.1	1.05	4.91063	4	4.9377	+0.6
1.10	3.02123	3	3.0108	-0.3	1.10	5.26356	5	5.2954	+0.6
1.15	3.28023	2	3.2749	-0.2	1.15	5.67710	3	5.6962	+0.3
1.20	3.58649	2	3.58901	+0.07	1.20	6.18157	3	6.2177	+0.6
1.25	3.97093	2	3.97471	+0.1	1.25	6.82447	3	6.8582	+0.5
1.30	4.48556	2	4.49332	+0.2	1.30	7.69076	4	7.7297	+0.5
1.35	5.23657	2	5.24896	+0.2	1.35	8.95834	3	9.0030	+0.5
1.40	6.49729	3	6.52200	+0.4	1.40	11.0842	4	11.139	+0.5
1.45	9.35970	2	9.35312	-0.07	1.45	15.8898	4	15.966	+0.5
1.46	10.5172	2	10.5202	+0.03	1.46	17.8287	4	17.911	+0.5
1.47	12.2163	2	12.2295	+0.1	1.47	20.6715	4	20.778	+0.5
1.48	15.0719	3	15.0915	+0.1	1.48	25.4430	5	25.567	+0.5
1.49	21.5308	3	21.5817	+0.2	1.49	36.2206	5	36.479	+0.7

*1 FEM solution with 50 elements and 129 nodes.
*2 Eigenvalue number.

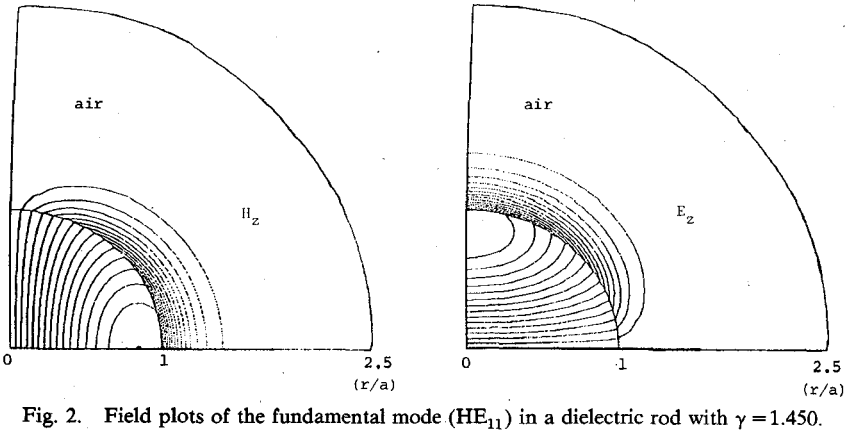

Fig. 2. Field plots of the fundamental mode (HE_{11}) in a dielectric rod with $\gamma = 1.450$.

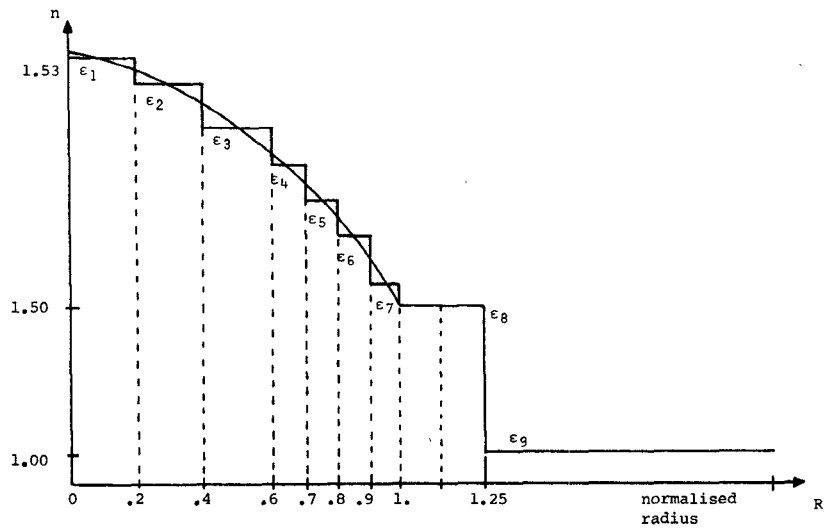

Fig. 3. The inhomogeneous optical fiber: Step index model of the parabolic profile.

TABLE III
NUMERICAL RESULTS FOR THE INHOMOGENEOUS OPTICAL FIBER

	HE_{11}			HE_{21}			HE_{31}		
γ	So(RK) *4	So(FEM) *1	% Error	So(RK) *4	So(FEM) *2	% Error	So(RK) *4	So(FEM) *3	% Error
1.04	0.977610	0.976640	-.100	2.170030	2.164290	-.260	3.20710	3.19167	-.48
1.10	1.187251	1.187124	-.011	2.389231	2.386839	-.100	3.458954	3.452893	-.180
1.14	1.311962	1.311868	-.007	2.545459	2.543810	-.065	3.652222	3.649044	-.087
1.20	1.510205	1.510257	+.003	2.819214	2.817969	-.044	4.003891	4.001578	-.058
1.24	1.662580	1.662602	+.001	3.043603	3.042554	-.034	4.299130	4.297761	-.032
1.30	1.949522	1.949422	-.005	3.485835	3.485218	-.018	4.891114	4.890539	-.012
1.34	2.208118	2.208048	-.003	3.898263	3.895336	-.075	-	5.447305	-
1.40	2.80/512	2.807164	-.012	4.885428	-	-	6.811314	6.807586	-.055

*1 Computed with 62 elements and 159 nodes in 1/4 fiber.
*2 Computed with 62 elements and 159 nodes in 1/8 fiber.
*3 Computed with 62 elements and 159 nodes in 1/12 fiber.
*4 Runge–Kutta solution computed in double precision.

For the fundamental mode, it is usually 1, except when a spurious mode is present (see Section IV-B).

The higher eigenvalues give the normalized frequencies of some of the higher order modes, but with an accuracy which falls very quickly because the rate of change of the field becomes very high and cannot be followed by the interpolation functions. For the next mode analyzed (HE_{12}), the accuracy degrades but stays below 0.08 percent over the γ-range (1.05–1.49). Other modes exist between HE_{11} and HE_{12} which cannot be found with the set of boundary conditions (imposed on the two axes of symmetry) which have been used in this example.

B. The Inhomogeneous Waveguide

The usual inhomogeneous fiber is circularly symmetric and has a slowly varying index of refraction in the radial direction (Fig. 3). One method of analysis uses a differential Runge–Kutta step by step approach [13]. Other methods can be found in [14]–[16]. Because it is a one-dimensional problem, the two-dimensional finite-element method is obviously not required for routine analysis, but the comparison between the results from these two methods constitutes an excellent test.

The step index model shown in Fig. 3 is used to approximate a parabolic profile and model a finite-cladding inhomogeneous fiber. Sixty-two elements and 159 nodes are generated to model the cross section. Table III gives the results from both methods for three modes and shows an excellent accuracy. The Runge–Kutta results were computed in double precision, but not the finite-element results because of the limited memory size of the minicomputer. At very low frequency, the field covers a large area outside the waveguide and the number of elements required to keep the accuracy constant must be greater. But the lower edge of the spectrum is not usually reached. For a typical free-space wavelength of 1 μm, a normalized frequency s equal to 1 corresponds to a normalizing a dimension of 0.16 μm, which is extremely small.

C. The Elliptical Waveguide

The elliptical fiber is described and analyzed with a different method in [17]. It has been selected for compari-

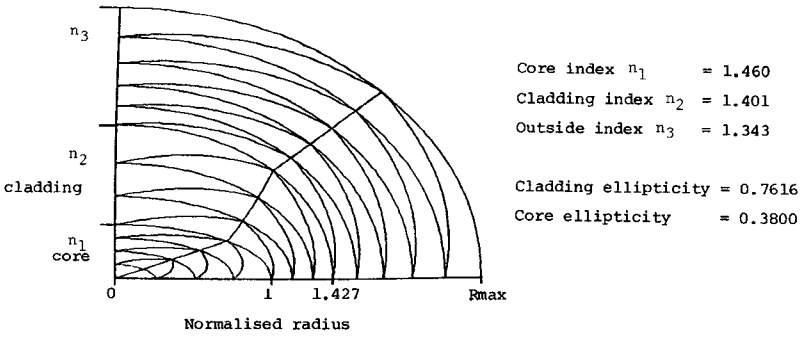

Fig. 4. Discretized cross section of the elliptical waveguide.

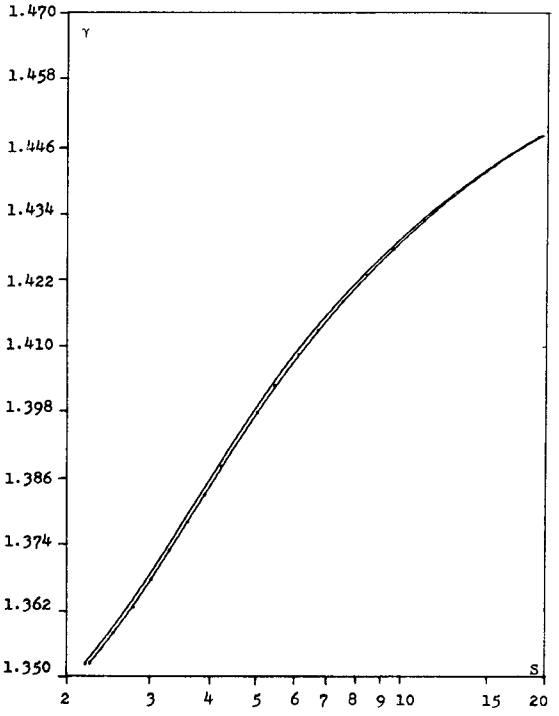

Fig. 5. Propagation characteristics of the first two modes of the elliptical fiber.

son and validation purposes, and because it is a truly two-dimensional problem.

This waveguide is made of three dielectric layers, the last one being infinitely wide. The two boundaries have a different ellipticity. (The ellipticity χ is defined such that any point (x, y) of the ellipse satisfied the following relations:

$$x = R\cos\phi,\ y = \chi R\sin\phi, \text{ and } 0 < \phi < 2\pi).$$

The virtual boundary is given the same ellipticity as the outer edge of the cladding. Fig. 4 shows one quarter of this structure.

The important result in this example is the so-called $\Delta\gamma$ characteristic curve (Fig. 6), which shows the very small gap between the propagation characteristics of the two lowest modes (Fig. 5). These are said to be quasi-degenerate and correspond to two different sets of boundary conditions.

The results from our method and from [17] exhibit a good agreement with a discretization made of only 46 elements and 119 nodes.

IV. Computational Remarks

A. Singularity

A theoretical limit of the formulation previously given in (1) is the singularity of τ_i when $\gamma^2 = \epsilon_i/\epsilon_0$. This can be seen more explicitly by rewriting (1) as (see [1])

$$\delta \sum_{i=1}^{N} \left\{ \int_{S_i} \tau_i \left[\phi_i \nabla_t^2 \phi_i + \gamma^2 \left(\frac{\epsilon_i}{\epsilon_0} \right) \psi_i \nabla_t^2 \psi_i \right] - k_0^2 \left(\phi_i^2 + \gamma^2 \frac{\epsilon_i}{\epsilon_0} \psi_i^2 \right) \right\} dS_i = 0 \quad (14)$$

where all the parameters have been previously defined in (1). When γ^2 approaches ϵ_i/ϵ_0, τ_i goes to infinity, but the Helmholtz equations become the static equation ($\nabla_t^2\phi_i = \nabla_t^2\psi_i = 0$) in each element i, and the products occuring in (11) are undefined.

One example has been studied (which can also be found in [18]) with a finite cladding fiber having three layers with a relative index of refraction of 1.53, 1.50, and 1.0, respectively, and a cladding to core dimensional ratio of 5. Only a few points of the fundamental mode propagation curve were computed, close to the singular value $\gamma = 1.50$. Numerical results obtained in single precision show a noticeable error when $|\gamma - (\epsilon_i/\epsilon_0)| < 0.002$ and, therefore, the results obtained inside this interval are not valid. Fig. 7 shows the effect of such a singularity.

B. Spurious Modes

A spurious mode is an eigenvalue–eigenvector pair of the numerical scheme which does not represent a real propagating mode in the waveguide. It has been observed by many authors [5], [7], [19]. Its detection may be very difficult when many modes have propagation characteristics close to each other. In the present work, spurious modes were identified by plotting the equipotentials of H_z or E_z, which tend to be smooth for true modes and jagged for spurious modes (Fig. 8).

C. The Eigenvalue Solver

The eigenvalue solver used to solve (13) used tridiagonalization and a Sturm sequence search. Eigenvectors were computed by inverse iteration. Problems of up to 250 degrees of freedom could be handled on a PERQ minicomputer, with around $\frac{1}{2}$ Mbyte of memory. A solver

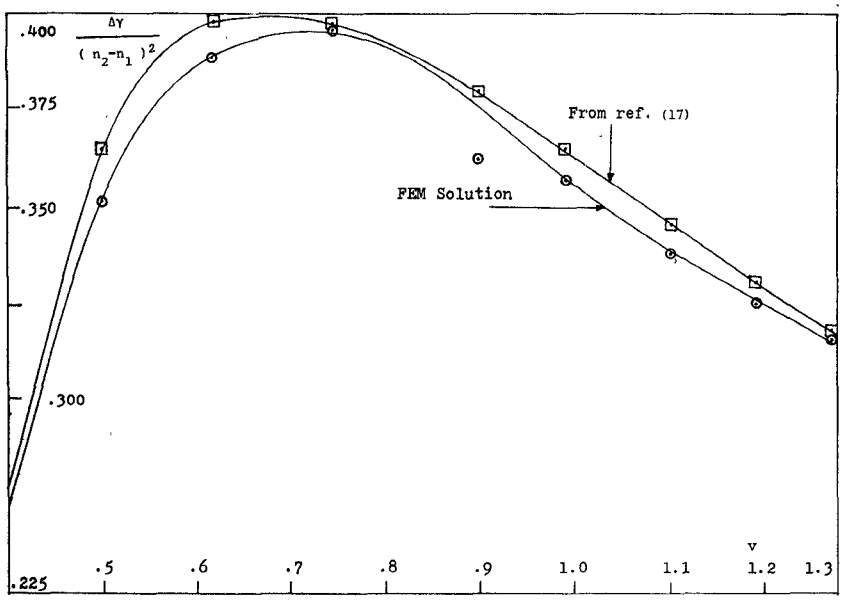

Fig. 6. Elliptical waveguide example: Difference between the propagation characteristics of the first two modes.

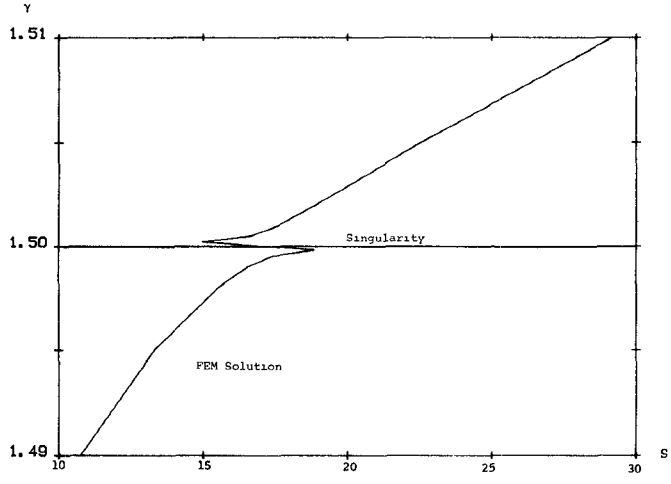

Fig. 7. Propagation characteristics of the fundamental mode near a singularity.

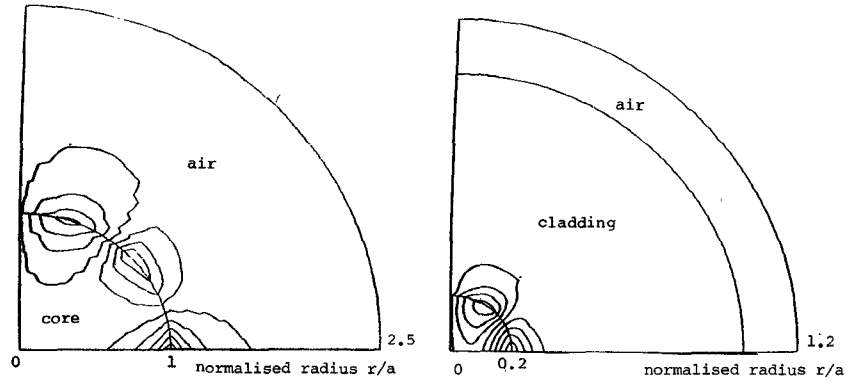

Fig. 8. Comparison between a real high-order mode and a spurious mode. Left: Spurious mode for a dielectric rod. Right: Real HE_{31} mode for a finite cladding fiber.

which took account of the sparsity of the matrices would extend considerably the size of the problem solvabie for a given amount of memory.

D. The Virtual Boundary

Outside the dielectric waveguide, and if there is no opaque coating, the electromagnetic field decays exponentially for a theoretically infinite distance. But it is obviously not possible to discretize this infinitely large area with a finite number of elements of finite size.

Some authors [4], [7] have used special elements in the unbounded region with intrinsically decaying interpolation functions. In this approach, the user has to guess the decaying factor with some accuracy to keep the result in an acceptable range. In our case, we use the same type of element everywhere in a finite region, and set both electric and magnetic fields to a true zero at a certain distance, on the so-called virtual boundary.

The determination of this boundary can be done iteratively with step by step moves, expecting a convergence of the eigenvalues for sufficiently large values of the boundary distance [19]. But this process is very costly in terms of computer time.

A better approach is to consider an equivalent simple model (the dielectric rod) for the arbitrarily shaped guide when it is seen for a relatively large distance. It is then possible to compute an approximate field decay rate to obtain the location of the virtual boundary. A separate program analyzes the dielectric rod with great accuracy. This method has been used successfully in the different cases studied in Section III.

The effect of the virtual boundary location on the accuracy of the answer has been numerically studied in one example. It shows an optimum range of values between which the results are very close to each other, within a so-called "numerical noise level." This expression refers to an apparent random variation of the eigenvalues with small variations of relatively irrelevant parameters.

When the boundary is too close, the approximation of the zero field leads to a fast-growing error. When the boundary is too far, the elements outside the waveguide become too large and the interpolation functions do not follow the fast decay rate.

V. The Monomode Optical Coupler Analysis

A. Description

The monomode optical coupler analyzed here is made of two monomode optical fibers stretched and fused together. As has been shown in [20] and [21], power can be exchanged between the two guides with a theoretically 100-percent efficiency when the cross-section dimension of the device becomes small enough. The phenomenon involved is not an evanescent wave coupling as obtained with other manufacturing techniques (e.g., by removing cladding material) but a mode beat effect [21], [9].

The loss of symmetry of the structure leads the fundamental mode splitting into four distinct mode with different propagation characteristics. Therefore, an accurate analysis of the device requires the accurate computation of the propagation characteristics of a complicated dielectric structure as it is shown in Fig. 9. This is achieved with the finite-element method.

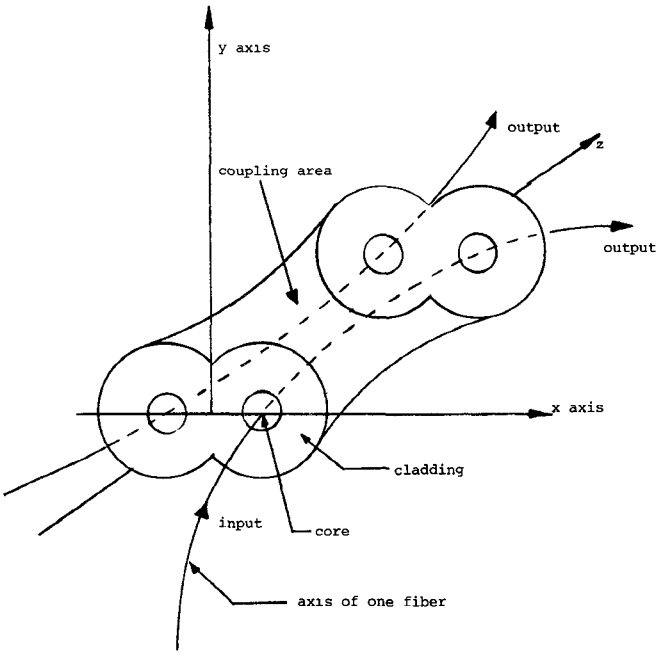

Fig. 9. Coupler geometry.

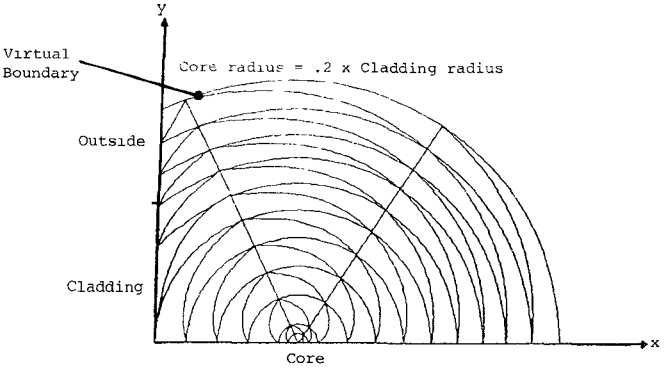

Fig. 10. Discretized cross section of one quarter of the coupler.

The four modes correspond to four sets of boundary conditions which may be imposed on the two geometrical axes of symmetry (defined as $0x$ and $0y$). (The reduction of the problem to a single quadrant and the subsequent definition of four sets of boundary conditions is a computational technique which increases the element density and the accuracy for a given cost.)

The four sets of boundary conditions are

	$(0x-\text{axis})$ $Ez=\psi=\varnothing$	$(0x-\text{axis})$ $Hz=\phi=\varnothing$
$(0y\text{-axis})$ $Ez=\psi=\varnothing$	4	3
$(0y\text{-axis})$ $Hz=\phi=\varnothing$	2	1

The lowest modes corresponding to these conditions are also labelled 1 to 4.

The geometry of the coupler is shown in Fig. 9, with a sample of the discretized cross section (one quadrant) shown in Fig. 10.

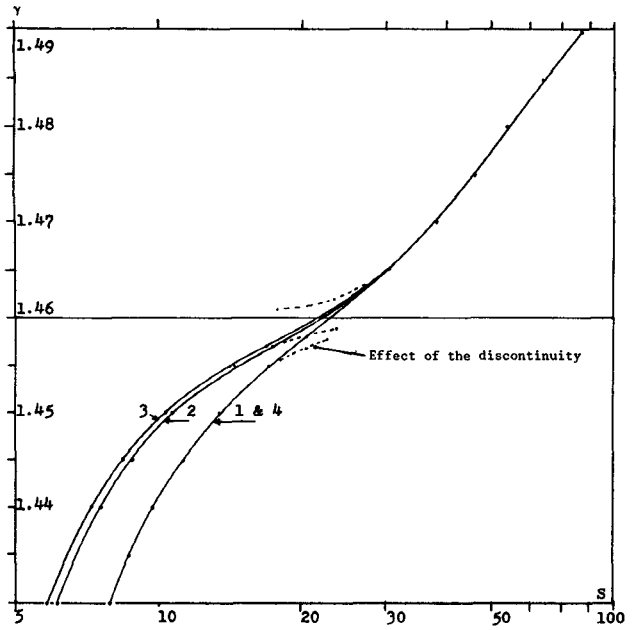

Fig. 11. Coupler Example 1): Propagation characteristics of the first four modes.

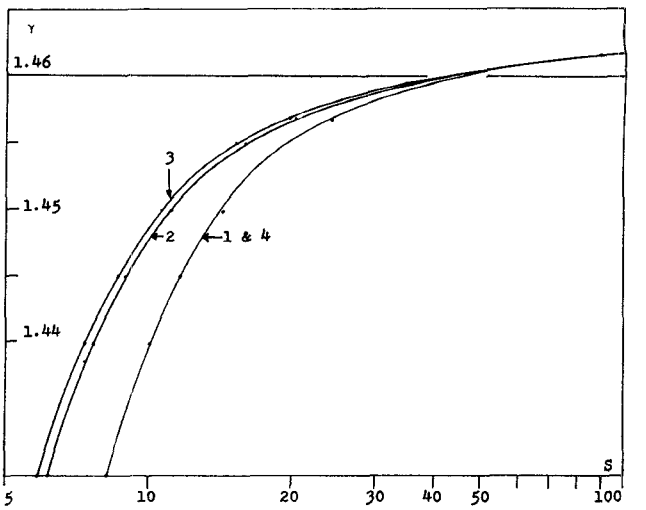

Fig. 12. Coupler Example 2): Propagation characteristics of the first four modes.

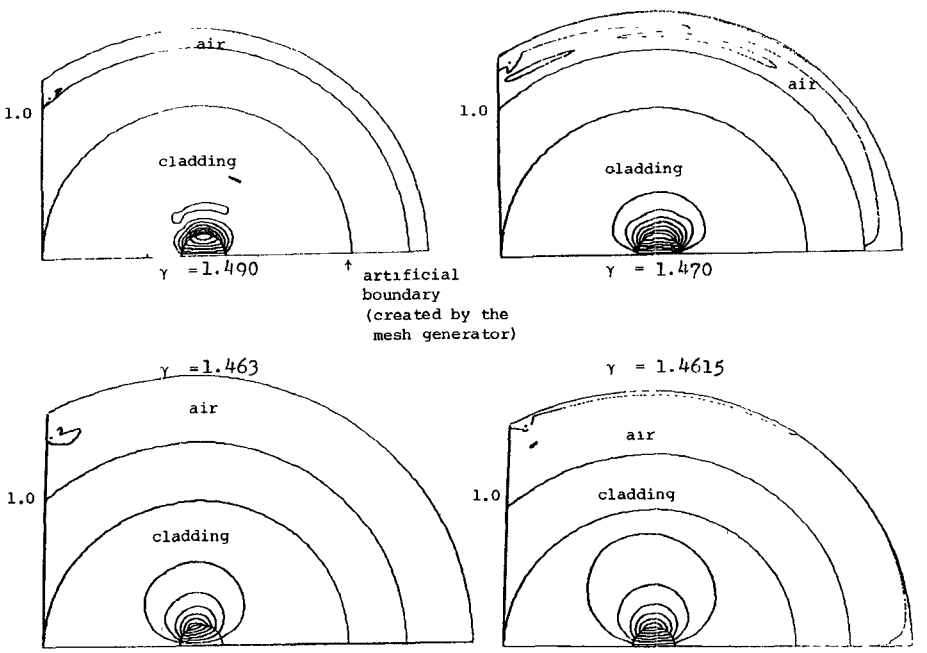

Fig. 13. Field plots of mode 2 in coupler 1 (E_z field) above cutoff.

The variation of the dimensions along the z-axis has been exaggerated on purpose. In fact, the taper is very gradual, and the coupler can be approximated with a set of very long guides with a constant cross section. In addition, we assume that the shape of the coupler is constant along the z-axis, all the dimensions changing with the same rate as the whole structure shrinks. Therefore, if the "a-dimension" is the radius of an individual fiber (the normalized frequency s being such that $s = \omega a/c$), the propagation characteristics of one mode inside the structure at any location along the longitudinal z-axis can be found simply by following the "γ versus s curve."

B. Results

Two couplers have been analyzed. The cladding index in both cases is 1.46, and the core index is 1.506 in the first example, and 1.4687 in the second example. The propagation characteristics of the first four modes are shown in Figs. 11 and 12. In both cases, the degeneracy of the four lower modes is very well observed for values of γ above the so-called cladding cutoff, e.g., when $\gamma > 1.46$, 1.46 being the refractive index of the cladding.

This behavior is related to a change in the field solution inside the cladding which becomes slowly nondecaying. It is equivalent to a change of the Bessel' s function type in

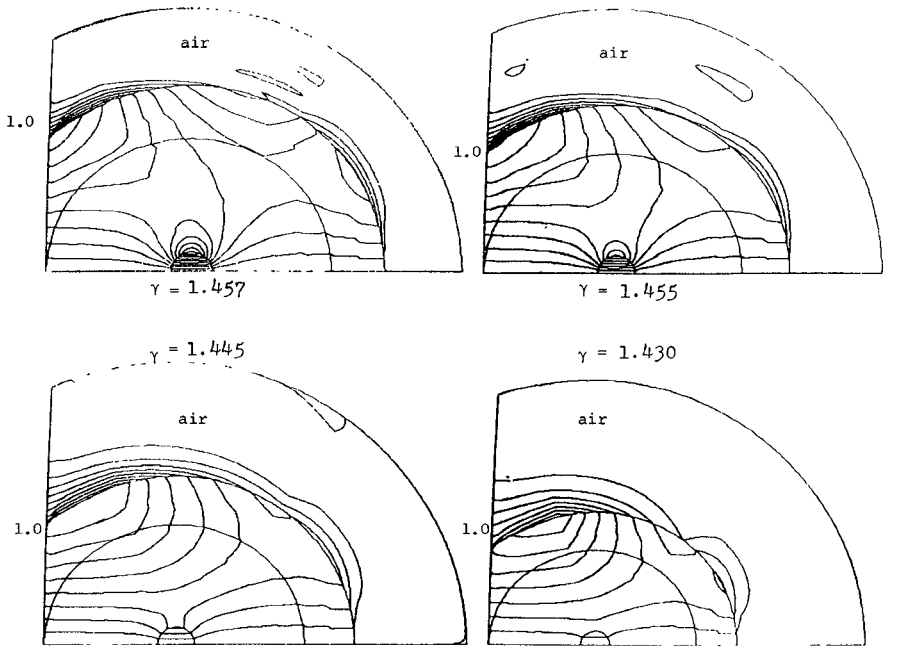

Fig. 14. Field plots of mode 2 in coupler 1 (E_z field) below cutoff.

the analysis of a finite cladding fiber [18]. The effect of the singularity at $\gamma = 1.46$ is avoided by ignoring the points in the γ-range (1.458–1.462).

The contours given in Figs. 13 and 14 associated with some of the γ-values selected previously show the effect of the degeneracy.

In Fig. 13, the field is concentrated in the core and is very similar to the field of an isolated fiber as it is shown in Fig. 2.

The end of the degeneracy is very fast when γ falls below 1.46, and the field fills the cladding. This corresponds to the coupling effect described in [20], when the superposition of the four nondegenerate modes gives a beat effect.

As expected, the end of the degeneracy in Example 2 occurs at a higher frequency (see Fig. 12) because the core index is closer to the cladding index. This gives a smoother transition than in the previous case. The smaller gap between the two indices allows the field to spread sooner into the cladding. At low γ, the two examples become similar, the importance of the core being negligible in the field distribution.

VI. Conclusion

The use of curved-sided (isoparametric) second-order finite elements has been shown to be an efficient and accurate means of analyzing dielectric waveguides with curved boundaries. This type of element is particularly suited to the study of monomode optical fiber devices.

References

[1] S. Ahmed and P. Daly, "Finite element method for inhomogeneous waveguides," *Proc. Inst. Elec. Eng.*, vol. 116, no. 10, pp. 1661–1664, Oct. 1969.

[2] Z. J. Csendes and P. Silvester, "Numerical solution of dielectric loaded waveguide: I—Finite-element analysis," *IEEE Trans. Microwave Theory Tech.*, vol. MTT-18, pp. 1124–1131, Dec. 1970.

[3] C. Yeh, S. B. Dong, and W. Oliver, "Arbitrarily shaped inhomogeneous optical fibers or integrated optical waveguides," *J. Appl. Phys.*, vol. 46, no. 5, p. 2126, May 1975.

[4] C. Yeh, K. Ha, S. B. Dong, and W. P. Brown, "Single-mode optical waveguides," *Appl. Opt.*, vol. 18, no. 10, pp. 1490–1495, May 15, 1979.

[5] N. Mabaya, P. E. Lagasse, and P. Vandenbulcke, "Finite element analysis of optical waveguides," *IEEE Trans. Microwave Theory Tech.*, vol. MTT-29, pp. 660–605, June 1981.

[6] J. Katz, "Novel solution of 2-D waveguides using the finite element method," *Appl. Opt.*, vol. 21, no. 15, pp. 2747–2750, Aug. 1, 1982.

[7] B. M. A. Rahman and J. B. Davies, "Finite element analysis of optical and microwave waveguide problems," *IEEE Trans. Microwave Theory Tech.*, vol. MTT-32, pp. 20–28, Jan. 1984.

[8] P. Daly, "Finite element approach to propagation in elliptical and parabolic waveguides," *Int. J. Numerical Methods in Engineering*, vol. 20, pp. 681–688, 1984.

[9] D. Welt, "A second order isoparametric finite element analysis of dielectric waveguides with curved boundaries," M. Sc. thesis, Dept. Elec. Eng., McGill University, Montreal, Apr. 1984.

[10] G. Dhatt and G. Touzot, *Une Presentation de la Methode des Elements Finis*, S. A. Maloine, Ed. Quebec and Paris: Les Presses de l'Universite Laval, 1981.

[11] O. C. Zienkiewicz, *The Finite Element for Engineering Sciences*, 3rd ed. New York: McGraw Hill, 1977.

[12] M. K. Barnoski, *Fundamentals of Optical Fiber Communications*, 2nd ed. New York: Academic Press, 1981, p. 16.

[13] G. L. Yip and Y. H. Amhew, "Propagation characteristics of radially inhomogeneous optical fibers," *Electron. Lett.*, vol. 10, no. 4, Feb. 21, 1974.

[14] H. H. Yao and G. L. Yip "Numerical study of inhomogeneous optical waveguide problems using predictor–corrector method," *Electron. Lett.*, vol. 17, no. 6, pp. 229–230, Mar. 19, 1981.

[15] Y. H. Ahmew, "Propagation characteristics of the self focusing fibre waveguide," M. Eng. thesis, Dept. Elec. Eng., McGill University, Montreal, Canada.

[16] M. S. Sodha and A. K. Ghatak, *Inhomogeneous Optical Waveguides*. New York and London: Plenum Press, 1971.

[17] S. R. Rengarajan and J. E. Lewis "Single mode propagation in multi-layer elliptical fiber waveguide," *Radio Sci.*, vol. 16, no. 4, pp. 541–547, July–Aug. 1981.

[18] J. Martucci, "Propagation and loss characteristics of cladded optical fibers," M. Eng. thesis, Dept. Elec. Eng., McGill University, Montreal, Canada, 1973.

[19] M. Ikeuchi, H. Sawamil, and H. Hiki, "Analysis of open-type dielectric waveguides by the finite-element iterative method," *IEEE Trans. Microwave Theory Tech.*, vol. MTT-29, pp. 234–239, Mar. 1981.

[20] J. Bures, S. Lacroix, and J. Lapierre, "Analyse d'un coupleur bidirectionnel a fibres optiques monomodes fusionnees," *Appl. Opt.*, vol. 22, pp. 1918–1922, June 15, 1983.
[21] A. W. Snyder, "Coupled mode theory for optical fibers," *J. Opt. Soc. Amer.*, vol. 62, no. 11, pp. 1267–1277, Nov. 1972.

✠

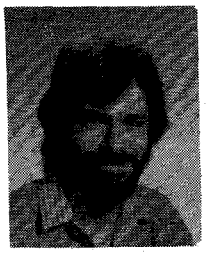

Daniel Welt was born in Paris, France, in 1957. He received the B. Ing. degree in electrical engineering from Ecole Polytechnique de Montréal, Québec, Canada, in January 1980, and the M. Eng. degree in electrical engineering from McGill University, Montreal, Canada, in the spring of 1985.

From February 1983 to November 1984, he worked with Antech Antenna Technologies Ltd., in Montreal. He designed various microwave satellite telecommunication components and implemented software for microwave network analysis. In December 1984, he joined MPB Technologies and is now developing patch antenna products.

His main topics of interest are electromagnetic-field numerical analysis and RF automatic measurement techniques.

✠

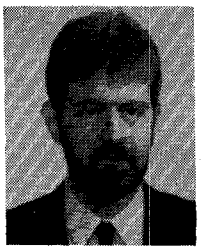

Jon Webb (M'83) obtained the Ph.D. degree from Cambridge University, England, in 1981, on a three-dimensional finite-element method for finding electromagnetic fields in cavities.

Since 1982, he has been an Assistant Professor in the Electrical Engineering Department at McGill University, Montreal, Canada. His area of research is numerical methods in electromagnetics.